JOURNAL OF APPLIED ELECTROCHEMISTRY 26 (1996) 853–863

Nucleation and crystal growth in gold electrodeposition from acid solution Part II: Hard gold

Y. G. LI, A. LASIA

Département de Chimie, Université de Sherbrooke, Sherbrooke, Québec, J1K 2R1, Canada

Received 14 August 1995; revised 25 January 1996

The mechanism of nucleation and crystal growth of hard gold (Au–Ni) on a gold rotating disc electrode from a proprietary bath (Renovel N) was investigated using linear sweep voltammetry and chronoamperometry. It was shown that two distinct mechanisms in two potential ranges are involved in this process. Experimental current–time transients at more positive potentials were described in terms of three-dimensional progressive nucleation and growth of right-circular cones. Time-independent inhibition of the vertical crystal growth was observed with an increase in negative potential, similar to the soft gold deposition. A modified inhibition model, in which vertical growth rate was assumed to decrease exponentially with time to a constant value, was derived to interpret experimental current–time transients recorded at more negative potentials. The chronoamperometric transients were well described by this model. Potential dependence of initial minima, maxima and final steady-state current was discussed.

1. Introduction

Two classifications of gold electrodeposits, that is, soft gold (pure gold) and hard gold, are extensively applied in the electronic industry. Soft gold has relatively poor wear resistance, therefore, its use in electronic connectors is limited. It has been well known for many years [1] that hard gold alloys may meet the combined requirements for low electrical contact resistance, low porosity, high corrosion resistance and high wear resistance. So-called hard gold alloys are usually codeposited with low quantities of metal hardener such as nickel, cobalt or iron [1–4]. Among the several gold plating systems, acid solutions are usually preferred for hard gold alloy plating [1, 5]. Publications dealing with the hard gold deposition were mostly confined to the properties and the morphology of deposit [6–22]. To the best of our knowledge, there are no publications on the mechanism of nucleation and crystal growth during initial stages of hard gold electrodeposition.

General electrochemical behaviour of soft and hard gold plating from Ronovel N baths was presented in our earlier paper [22]. In Part I [23], electrocrystallization kinetics of soft gold was investigated. It was found that at more positive potentials reaction proceeds via three-dimensional (3D) progressive nucleation and crystal growth mechanism (with some contribution of progressive 2D process) and at more negative potentials according to 3D instantaneous nucleation mechanism. Besides, self-inhibition of crystal growth was observed at some potentials. The aim of the present paper is to study the mechanism of nucleation and crystal growth during hard gold electroplating and to compare it with soft gold deposition. The morphology of deposit was also examined.

2. Theoretical aspects of nucleation and crystal growth

After nucleation, lone crystal centres grow via different growth modes, for example, two-dimensional cylindrical growth, three-dimensional growth of right-circular cones, hemispheres etc. In the derivation of current–time equations the problem of the overlap of growing crystals was taken into account using Arami's theorem [24] and Evans' method [25]. Several models concerning nucleation and crystal growth phenomena have been developed for different cases [26–28]. For instance, a hemispherical growth model [26, 27] may be used to explain the formation of a peak and a plateau on current–time transients, which are usually observed during electrocrystallization of nickel [29]. The ratio of the peak to the plateau currents is expected to be 1.285 for instantaneous nucleation or 1.333 for progressive nucleation [26, 27]. In other experiments [30, 31], although a similar shape of current–time transients was observed the ratio of the peak to the plateau current was much higher than values presented above. Hence, this model could not well explain such experimental phenomena. It is well known that the crystal growth at later stages may be determined by overlapping of crystals and also other unknown nuclei death process. The later factor results in the time-dependence of growth rate in a particular direction (e.g., in the case of inhibition process). Armstrong *et al.* [32] were the first to develop

0021-891X

a model of nucleation and growth with passivation, in which the vertical growth rate was assumed to be proportional to the free surface area uncovered by growing crystals. Current for 3D progressive nucleation in this passivation model is given by [32]

$$i = zFk'\left[1 - \exp\left(-\frac{\pi M^2 k^2 A_{3D}}{3\rho^2} t^3\right)\right] \times \exp\left(-\frac{\pi M^2 k^2 A_{3D}}{3\rho^2} t^3\right) \quad (1)$$

where k' and k are growth rate constant in the direction perpendicular and parallel to the substrate (mol cm^{-2} s^{-1}), respectively, A_{3D} nucleation rate (nuclei cm^2 s^{-1}), ρ is the deposit density, M its molecular mass, and other symbols have their usual meaning. In this case current first increases with time and then, at longer times, decreases to zero. This model has been modified by Barradas *et al.* [33] by inclusion of a time-independent constant x in Equation 1:

$$i = zFk'\left[1 - \exp\left(-\frac{\pi M^2 k^2 A_{3D}}{3\rho^2} t^3\right)\right] \times \left[\exp\left(-\frac{\pi M^2 k^2 A_{3D}}{3\rho^2} t^3\right)\right]^x \quad (2)$$

Although current, according to Equation 2, still decreases to zero at longer times, the shape of current–time transients may be changed by the parameter x. However, Bosco and Rangarajan [26] found that the original passivation model described by Equation 1 is incorrect. They developed a general model of nucleation and crystal growth. In the case of vertical growth with inhibition, the vertical growth rate constant, k', was assumed to be time dependent:

$$k' = k_1 \exp(-\lambda t^n) \quad (3)$$

where n is 1 to 3, and k_1 and λ are constants. For $n = 1$, the current for instantaneous nucleation is described by [26]:

$$i = zFk_1\left[\exp(-\lambda t) - \exp(-P_2 t^2) + \lambda \exp(-\lambda t)\int_0^t \exp(-P_2 u^2 + \lambda u)\mathrm{d}u\right] \quad (4)$$

where $P_2 = \pi M^2 k^2 N_0/\rho^2$, N_0 is the total number of active centres per cm^2, other symbols have been defined above. Equation 4 and other models taking into account inhibition process, described in [26], predict that current increases with time to a maximum and then decreases to zero at longer times.

If the product adsorbed on the surface acts as an insulator, current should decrease to zero at long times, when the surface of electrode becomes completely covered. This was observed for anodic oxidation of mercury [32]. However, for the case of partial surface coverage by an inhibitor, current would be expected to decrease and then reach a plateau. Therefore, in such a case, we propose a more general form of time-dependence of vertical growth rate constant:

$$k' = k_1 \exp(-\lambda t^n) + k_2 \quad (5)$$

where k_2 is a constant. The rate constant of vertical growth changes from $k_1 + k_2$ at $t = 0$ to k_2 at $t \to \infty$. Modified inhibition models may be derived using a general method presented in [26]. Assuming that (a) nucleation is instantaneous; (b) lateral growth velocity k (mol cm^{-2} s^{-1}) is constant and (c) growth in vertical direction is partially inhibited and vertical growth velocity k' is given as

$$k' = k_1 \exp(-\lambda t) + k_2 \quad (6)$$

then equation describing dependence of current on time may be derived as (see Appendix A):

$$i = zFk_1\left[\exp(-\lambda t) - \exp(-P_2 t^2) + \lambda \exp(-\lambda t)\int_0^t \exp(-P_2 u^2 + \lambda u)\mathrm{d}u\right] + zFk_2[1 - \exp(-P_2 t^2)] \quad (7)$$

It should be noticed that current in Equation 7 consists of two terms, the first one is the same as Equation 4 in which vertical growth rate was assumed to decrease with time to zero, and second one is the same as the equation derived by Armstrong *et al.* [32] for 3D instantaneous nucleation and growth of right-circular cones with vertical growth rate constant of k_2. The modified inhibition model, Equation 7, predicts that after nucleation current increases with time to a maximum and then decreases to a steady-state value ($i_{ss} = zFk_2$) at longer times. The ratio of the peak to the steady-state currents depends on various parameters of the process, as illustrated in Fig. 1. It is obvious that if k_1 or λ equals zero this model simplifies to a 3D instantaneous nucleation and growth of right-circular cones [32], whereas when k_2 equals zero, it corresponds to the case of complete inhibition of vertical growth, Equation 4.

Other models for partial vertical growth inhibition based on Equation 5 may be similarly derived (see Appendix B, for $n = 2$ in Equation 5). It may be shown that in all cases of a partial vertical growth inhibition, current would be expected to increase to a maximum and then reach a steady-state value at

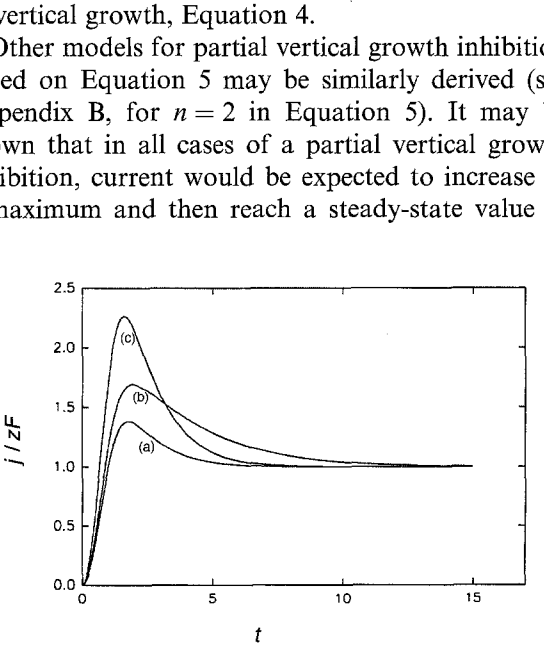

Fig. 1. Simulated current–time transients according to Equation 7: (a) $k_1 = k_2 = P_2 = \lambda = 1$, (b) $k_1 = k_2 = P_2 = 1$, $\lambda = 0.5$, (c) $k_2 = P_2 = \lambda = 1$, $k_1 = 3$.

longer times. However, shape of the transients depends on the parameters in Equation 5.

3. Experimental details

Hard gold plating bath (solution D) used in this study consisted of three components:

(i) the proprietary supporting electrolyte (Renovel N make-up solution, Lea Ronal);
(ii) the proprietary nickel containing solution (Renovel N nickel concentrate, Lea Ronal);
(iii) gold cyanide $KAu(CN)_2$ (SEL–REX, Enthone–OMI).

Renovel N make-up solution is a citrate-based buffer solution containing nicotinamide as a current density extender [9]. The bath used consisted of 75% (by volume) of component (i), the concentration of gold was 0.091 M and that of nickel 0.029 M. The pH of the solution was adjusted to 4.4. Working temperature was $60 \pm 0.5\,^{\circ}C$. Detailed electrochemical procedure was given in Part I [23].

The morphology of deposits was examined with a JSM–840A scanning electron microscope (SEM). For SEM studies, gold-plated nickel rotating disk electrode (RDE) (diam. 3.0 mm) was used. Nickel RDE was polished with 0.1 μm Al_2O_3, rinsed thoroughly with water, kept in H_2SO_4 (1 : 2) for 15 s and finally washed with deionized water. Pure (soft) gold layer was plated on the nickel RDE from an alkaline gold solution ($KAu(CN)_2$ 40 g dm^{-3} KCN 7.5 g dm^{-3} and KOH 40 g dm^{-3}) at 1000 rpm and $i = 7.5$ mA cm^{-2} for 50 s, its surface was checked by SEM to be very smooth and uniform. Samples of hard gold deposit for SEM were obtained after hard gold deposition on the soft gold-plated nickel RDE from solution D.

4. Results

4.1. *Linear sweep voltammetric measurements*

A linear sweep voltammogram (LSV) of hard gold deposition on the gold RDE from solution D is shown in Fig. 2, line b. LSV for soft gold deposition (without addition of nickel) is also presented in Fig. 2, line a. Current for hard gold deposition starts to increase at about −0.35 V. Similarly to soft gold deposition, two potential regions on LSV are clearly seen. At more positive potentials (from −0.5 to −0.725 V), a characteristic current peak appears. The peak is affected by pH of solution, for example, current density at peak increases about 20% as pH changes from 4.0 to 4.4. It is unlikely that this peak is caused by the hydrogen evolution reaction (HER) because such current should increase with a decrease of pH [34].

Inhibition of hard gold deposition occurs in this potential range, in an agreement with the finding for soft gold deposition [23]. Besides, current for hard gold deposition is much smaller than that for soft gold. The current peak on LSV is shifted into more positive direction, as compared with soft gold deposition. In the second potential range (from −0.725 to −1.0 V), current increases abruptly as potential becomes more negative. This may correspond to the deposition of gold via a direct charge-transfer mechanism simultaneously with HER.

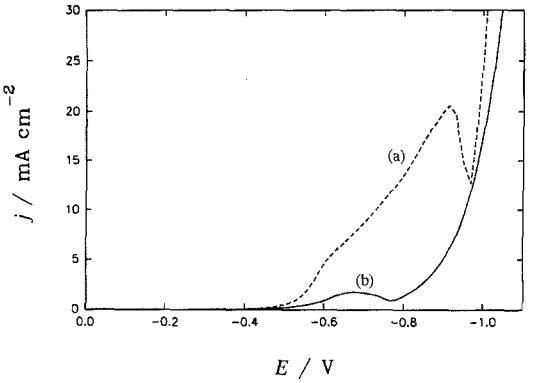

Fig. 2. Linear sweep voltammograms obtained on a gold rotating disc electrode for soft gold (a) and hard gold (b); sweep rate: 1 mV s^{-1}; rotation speed: 650 rpm.

As discussed in Part I [23], current peak on LSV might be caused by an inhibitor produced during the electroreduction reaction and the removal of the inhibitor from surface to bulk solution may be under mass transfer control. In fact, current peak on LSV at a scan rate of 1 mV s^{-1} in solution D disappeared when a stationary electrode was used, indicating that the deposition process of gold was completely inhibited in the absence of forced mass transfer.

4.2. *Chronoamperometric measurements*

Measurements under stationary conditions were not carried out because they led to relatively long transients, up to a few hours, recorded in first potential range. This observation indicates that the nucleation and growth processes were strongly inhibited. In order to decrease the influence of mass transfer on the deposition, all chronoamperometric measurements were performed under rotation rate of 4000 rpm.

Figure 3 displays a typical set of current-time transients for hard gold deposition from solution D in a wide potential range. The shape of transients was different from that for soft gold deposition, especially at more negative potentials. It is clear that different shape of current transients indicates different nucleation and growth mechanisms. At more positive potentials (from −0.5 to −0.725 V), the behaviour of current–time transient is somewhat similar to that of soft gold, that is, after the initial fast decrease, current increases with time due to nucleation and crystal growth, and then reaches a quasi-plateau. The quasi-plateau current increases with an increase in negative potential, reaches a maximum at −0.55 V and then decreases until potential of −0.70 V, which is probably caused by an inhibition process [23]. Similar to soft gold deposition, the initial current minimum increases as potential becomes more negative. The fact that the current for hard gold deposition is much lower than that for soft gold indicates that

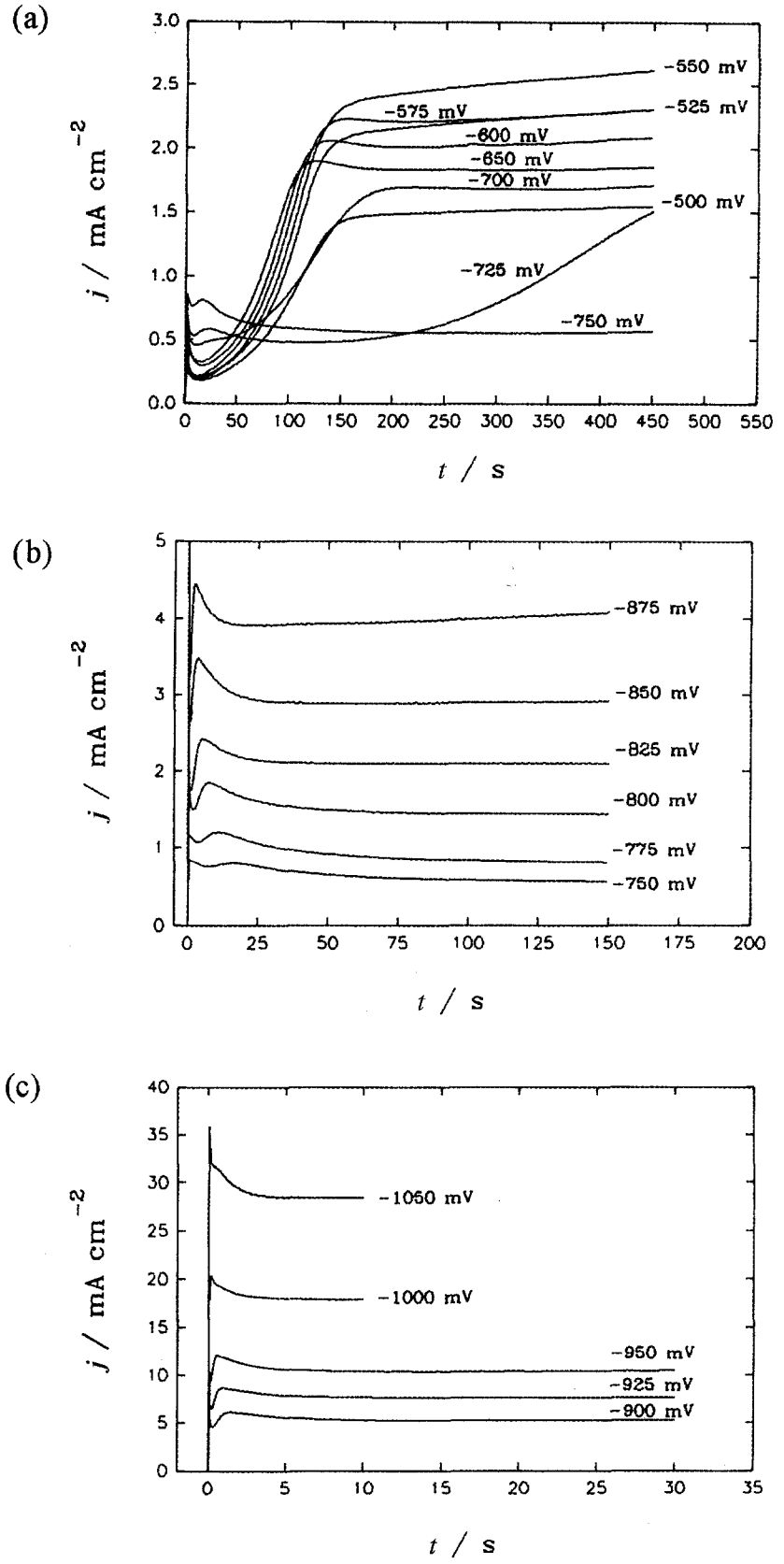

Fig. 3. Experimental current–time transients for hard gold deposition on Au RDE; rotation speed: 4000 rpm.

crystal growth is inhibited by the presence of nickel. At more negative potentials between −0.725 V and −1.0 V, after the initial fall, current increases to a maximum and then decreases with time to a steady-state. Current values at minima, maxima and steady-state conditions in this potential range increase with negative potential, and Tafel plots based on these current values show similar slopes, Fig. 4. These current values also increase with the rotation rate (not shown here). It is most likely that such a shape of current transients is not determined by a mass transfer of gold cyanide because the observed current is much lower than the diffusion limited one predicted by Levich equation.

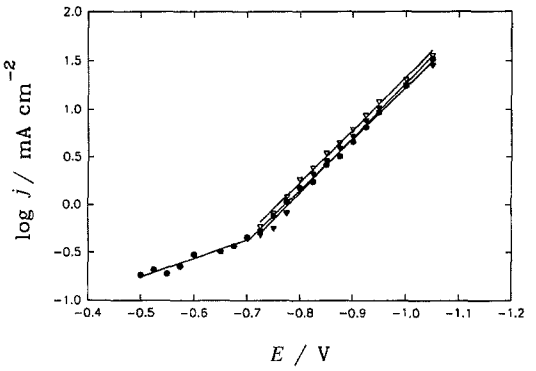

Fig. 4. Tafel plots constructed on the basis of the initial minimum (●), maximum (▽) and steady-state current (▼), shown in Fig. 3, for hard gold deposition.

As discussed in Part I [23], current recorded at longer times under potentiostatic conditions, in the case of electrocrystallization with an inhibition, could not be used to construct Tafel plots. However, the initial minimum current was suitable to be used for such a purpose. This was further confirmed for hard gold deposition. A Tafel plot based on the initial current minima is displayed in Fig. 4 for hard gold deposition. It shows two linear regions with two different slopes of 0.47 V dec^{-1} in the range from −0.50 to −0.75 V and 0.18 V dec^{-1} at potentials between −0.75 V and −1.1 V. These values are in a good agreement with the results obtained by chronopotentiometric measurement, for which Tafel plots were based on the initial potential peak presented on the potential–time transient [22]. It should be noticed that the Tafel slope for hard gold deposition is higher than that for soft gold. Such relatively high Tafel slope may correspond to the adsorption of an intermediate, especially at lower overpotentials.

5. Discussion

5.1. *Mechanism of hard gold deposition*

The results obtained above are, in principle, similar to those obtained for soft gold deposition, in which adsorption of AuCN was followed by the electron-transfer at more positive potentials:

$$Au(CN)_2^- + H^+ \rightleftharpoons AuCN_{ads} + HCN \quad (8)$$

$$AuCN_{ads} + H^+ + e^- \rightarrow Au + HCN \quad (9)$$

and a direct charge-transfer mechanism under higher overpotentials:

$$Au(CN)_2^- + 2H^+ + e^- = Au + 2HCN \quad (10)$$

Therefore, the Tafel slope obtained at more negative potentials would be expected to be lower than that obtained at more positive potentials because the actual charge transfer, in the case of specific adsorption, occurs to species in the inner Helmholtz plane [20]. For deposition at more positive potentials, the production of CN^- or HCN on the electrode surface leads to the shift of the chemical adsorption reaction, Equation 8, to the left. This results in a self-inhibition effect, as discussed in part I [23].

Higher Tafel slopes for hard gold deposition may be related to the presence of nickel. The deposition current for hard gold is much lower than that for soft gold. Although nickel contents in deposits is only about 0.3%, the nucleation and growth mechanism is modified by its presence. The growth of gold crystals may be inhibited because a part of active sites is occupied by nickel adatoms. This results in a decrease of gold crystal growth rate. Current efficiency of hard gold deposition on Pt RDE at longer times is about 50–75% [22]. The HER may be preferred on growing crystals containing nickel. It is possible that both nickel adsorbate and H adatom influence the mechanism of nucleation and crystal growth, especially at more negative potentials.

5.2. *Approximations of current–time transients: nucleation and crystal growth models*

As illustrated in Fig. 3, two different shapes of current-time transients are observed for hard gold deposition, which correspond to two distinct nucleation and crystal growth mechanisms. At potentials between −0.5 V and −0.70 V, the plateau-like behaviour may result from the 3D nucleation and crystal

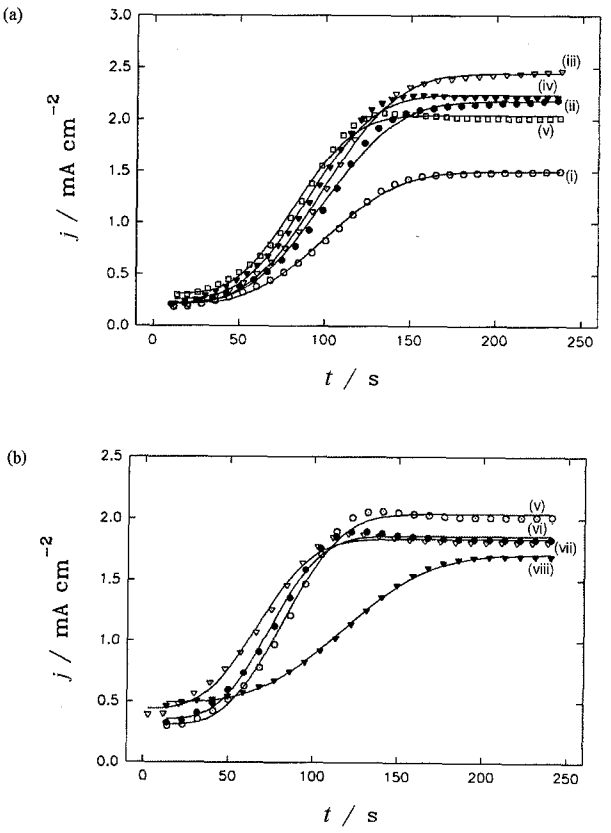

Fig. 5. Initial portion of current–time transients shown in Fig. 3 at potentials between −0.500 V and −0.700 V. Points: experimental data; solid line: theoretical fit to Equation 11. Potential: (i) −500, (ii) −525, (iii) −550, (iv) −575, (v) −600, (vi) −650, (vii) −675 and (viii) −700 V.

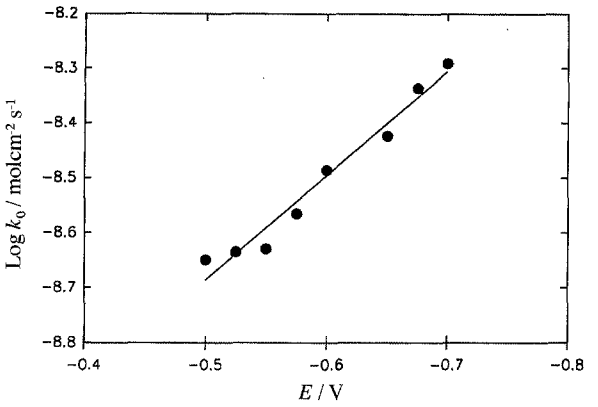

Fig. 6. Plot of $\log k_0$, determined from Equation 11, against potential applied for hard gold deposition at potentials between −0.5 and −0.7 V.

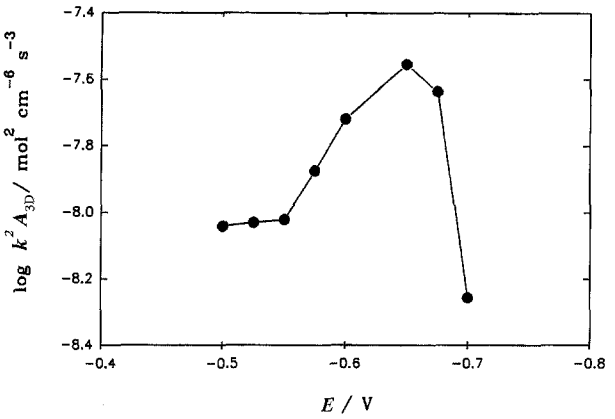

Fig. 8. Plot of $\log k^2 A_{3D}$, Equation 11, against potential applied for hard gold deposition at potentials between −0.5 and −0.7 V.

growth of right-circular cones. To fit these transients, it was assumed that three dimensional nucleation is progressive, similarly as for soft gold deposition [23]. Then, growth current consists of two parts [23]:

$$i = zFk_0 \exp\left(-\frac{\pi M^2 k^2 A_{3D}}{3\rho^2} t^3\right) + zFk'\left[1 - \exp\left(-\frac{\pi M^2 k^2 A_{3D}}{3\rho^2} t^3\right)\right] \quad (11)$$

where k_0 is the outward growth rate constant for substrate's base plane, A_{3D} is the nucleation rate constant and other symbols were described earlier. The first term in Equation 11 corresponds to the current for the growth of the substrate's base plane on a free surface area uncovered by growing crystals, and the second one due to the growth of right-circular cones. Figure 5 shows approximations of the experimental data by Equation 11, the fit is very good.

Kinetic information on crystal growth process may be estimated from the parameters derived. As discussed in Part I [23], zFk_0 in Equation 11 is interpreted as the initial current minimum on the current–time transient. Figure 6 gives a linear Tafel dependence of $\log k_0$ on potential. Hence, it is reasonable to construct a Tafel plot based on the initial minimum. The dependence of the vertical growth rate constant, k', on potential is shown in Fig. 7. It increases as potential changes from −0.50 to −0.550 V, whereas it decreases with negative potential in the range of potentials from −0.550 to −0.70 V. This suggests that vertical growth of crystals is inhibited, in consistent with the finding obtained from soft gold [23], where it was supposed that an inhibitor is produced on the electrode surface. Furthermore, the value of k' for hard gold is much smaller than that for soft gold. The combined rate constant, $k^2 A_{3D}$, initially increases and then decreases with negative potential, as shown in Fig. 8. Contrary to the dependence found for soft gold, the nucleation rate A_{3D} for hard gold deposition at more positive potentials, between −0.525 V and −0.675 V, seems to increase with negative potential applied, Fig. 9, provided that lateral and vertical growth rate constants are equal to each other. The plot of $\log A_{3D}$ against potential is a straight line, Fig. 9, in a good agreement with the prediction of the atomistic nucleation theory [35, 36].

The nucleation and crystal growth process for hard gold deposition at potentials between −0.750 V and −1.0 V is more complex. No simple model published in literature could describe the complete current-time transient recorded in this potential range. A few more complex models, for example, combined 2D and 3D nucleation/growth of right-circular cones,

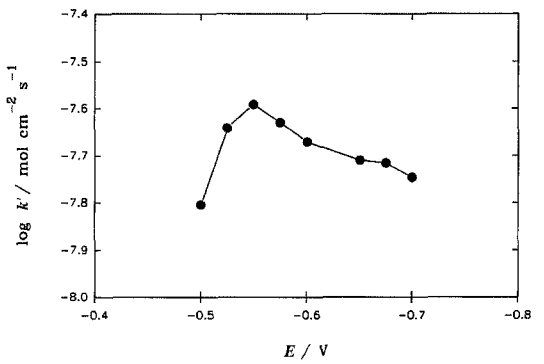

Fig. 7. Plot of $\log k'$, Equation 11, against potential applied for hard gold deposition at potentials between −0.5 and −0.7 V.

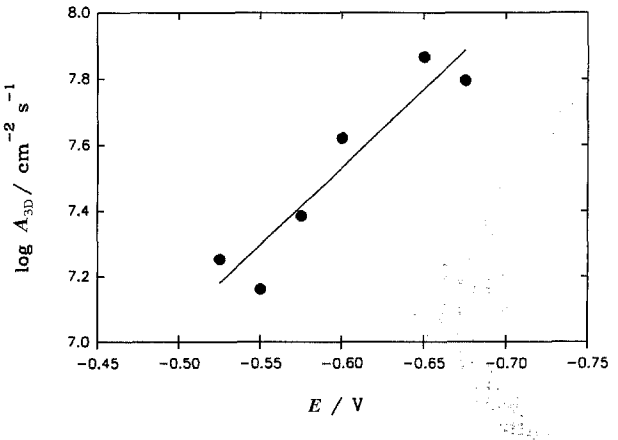

Fig. 9. Plot of $\log A_{3D}$, Equation 11, assuming that growth rate constants in vertical and lateral directions are equal, against potential applied for hard gold deposition at potentials between −0.5 and −0.7 V.

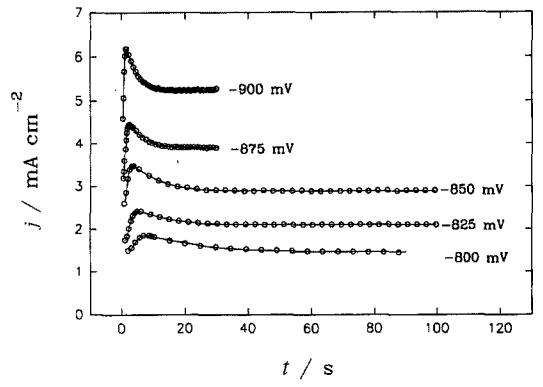

Fig. 10. Theoretical fit of experimental transients to Equation 12 for hard gold deposition from solution D at potentials more negative than −0.750 V. Points: experimental data; solid line: fitted. The parameters derived are shown in Table 1.

hemispherical or ellipsoidal growth [27], 3D nucleation and growth of right-circular cones with passivation [32], could not reproduce the correct shape of current–time transient. It should be noticed that after maxima, current decreases exponentially with time, and reaches a steady-state value at longer times, which is still potential dependent (see Fig. 3). An exponential decay of current with time following maxima was also assumed by Fleischmann *et al.* [37] to describe the death of crystal growth. Besides the effect of overlap of adjacent growing centres, the growth of centres at later stages of electrocrystallization could be largely determined by certain not yet known death processes. The adsorption of an inhibitor on the electrode surface would block the active sites available for nucleation and growth, and result in an abrupt cease of growth of nuclei (or death of nuclei). In order to describe the current–time transients recorded in potential range of −0.75 to −1.0 V, it was assumed that (i) 3D nucleation is instantaneous; (ii) vertical growth velocity, k', decreases exponentially with time and reaches a constant at longer times, according to Equation 4; (iii) lateral growth rate constant, k, is time-independent; (iv) to describe the initial minima recorded on current transients, outward growth of substrate's base plane was also taken into account. Therefore, the observed current consists of two parts, the first one due to outward growth of substrate's base plane and the second one due to instantaneous nucleation and 3D growth with a partial inhibition, Equation 7. The obtained equation may be represented as

$$i = P_0 \exp(-P_2 t^2) + P_1 \left[\exp(-\lambda t) - \exp(-P_2 t^2) + \lambda \exp(-\lambda t) \int_0^t \exp(-P_2 u^2 + \lambda u) \mathrm{d}u\right] + P_3 [1 - \exp(-P_2 t^2)] \quad (12)$$

where $P_0 = zFk_0$, $P_1 = zFk_1$ and $P_3 = zFk_2$, other symbols have been defined previously. It is clear from Equation 12 that at $t = 0$, $i = zFk_0$ and as $t \to \infty$, $i = zFk_2$. Equation 12 predicts that current initially increases from a minimum to a maximum and, subsequently, decreases to a steady-state value at longer times. The minimum current may be smaller or larger than the steady-state one, depending on the magnitude of k_0 and k_2. This model can be used to explain both initial minima and final steady-state on current–time transients shown in Fig. 3.

Figure 10 presents approximations of the experimental transients by Equation 12. It is evident that experimental data are very well approximated by the proposed model. The parameters derived are displayed in Table 1. The dependence of the rate constants k_0 and k_2 on potential are illustrated in Fig. 11. Linear Tafel relationships were obtained for both constants with similar slopes. The obtained results indicate that Tafel plots at potentials between −0.75 to −1.0 V may be constructed using the initial minimum or steady-state current. Though the dependence of $\log k_1$ on potential is also linear (Fig. 12), the slope of 0.26 V dec^{-1} is higher than that based on the initial current minimum. From Fig. 4, however, it can be seen that the Tafel slope based on the current maximum is the same as that based on the initial current minimum. This result indicates that the maximum is not only determined by the rate constant k_1 but also by other parameters. The dependence of the combined rate constant $k^2 N_0$ on potential is given in Fig. 13. This parameter increases with negative potential. Since lateral growth rate constant, k, is unknown, N_0 can not be estimated. The inhibition parameter λ increases with negative potential but its values are always smaller than 1 in our measurement, as shown in Fig. 14.

It should also be added that other effects like HER

Table 1. Kinetic parameters of hard gold deposition derived from the nonlinear least-squares fit of experimental j/t curves to Equation 12

Potential /V	P_0 /mA cm^{-2}	P_1 /mA cm^{-2}	P_2 /s^{-2}	λ /s^{-1}	P_3 /mA cm^{-2}
−0.750	0.685 ± 0.016	0.303 ± 0.006	0.011 ± 0.001	0.048 ± 0.001	0.571 ± 0.001
−0.775	1.147 ± 0.008	0.368 ± 0.006	0.128 ± 0.026	0.069 ± 0.002	0.900 ± 0.002
−0.800	1.506 ± 0.002	0.438 ± 0.003	0.123 ± 0.003	0.097 ± 0.001	1.467 ± 0.002
−0.825	1.723 ± 0.003	0.391 ± 0.004	0.222 ± 0.003	0.159 ± 0.002	2.104 ± 0.001
−0.850	2.635 ± 0.007	0.652 ± 0.006	0.683 ± 0.012	0.190 ± 0.003	2.893 ± 0.002
−0.875	3.083 ± 0.021	0.676 ± 0.006	1.053 ± 0.039	0.347 ± 0.004	3.913 ± 0.002
−0.900	4.506 ± 0.027	1.098 ± 0.019	2.811 ± 0.137	0.486 ± 0.004	5.253 ± 0.002
−0.925	6.303 ± 0.013	1.157 ± 0.007	9.269 ± 0.260	0.575 ± 0.007	7.654 ± 0.003
−0.950	9.377 ± 0.029	1.710 ± 0.012	23.47 ± 1.18	0.806 ± 0.008	10.44 ± 0.004

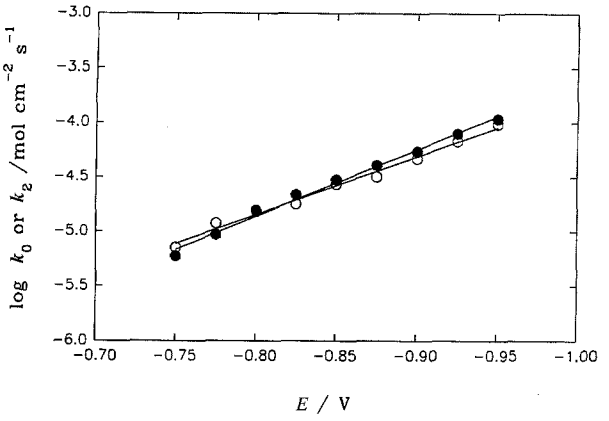

Fig. 11. Dependence of k_0 (○) and k_2 (●), determined from Equation 12, on potential applied for hard gold deposition at potentials more negative than −0.750 V.

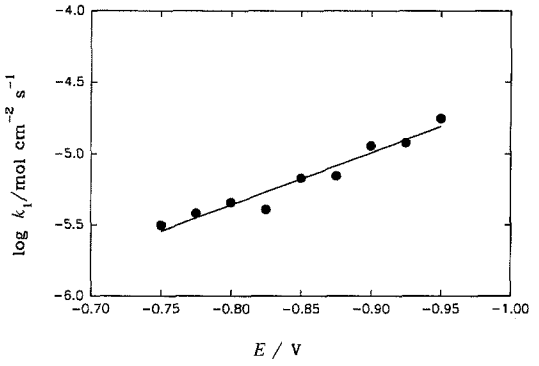

Fig. 12. Dependence of k_1, Equation 12, on applied potential for hard gold deposition at potentials more negative than −0.750 V.

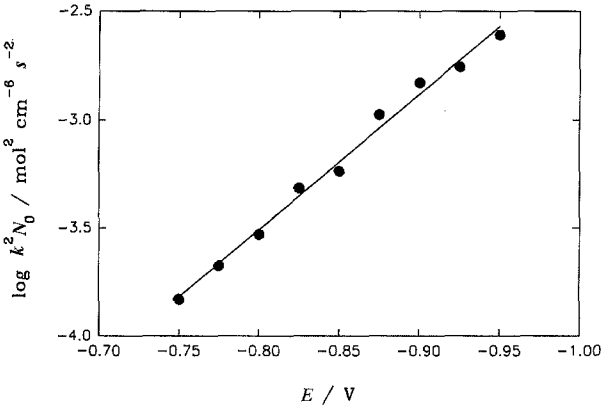

Fig. 13. Dependence of log (k^2N_0), Equation 12, on applied potential for hard gold deposition at potentials more negative than −0.750 V.

are ignored in Equation 12. However, the HER is important at very negative potentials only. Its effect can be taken into account using an approach similar to that presented by Abyaneh and Fleischmann [38]. In this case parameters P_0, P_1 and P_3 would be increased by a constant term including the rate constant of hydrogen evolution.

Although experimental data are well described by Equation 12, the physical meaning of this model is still not clear. It is unknown what causes the exponential decrease of growth rate to a constant value.

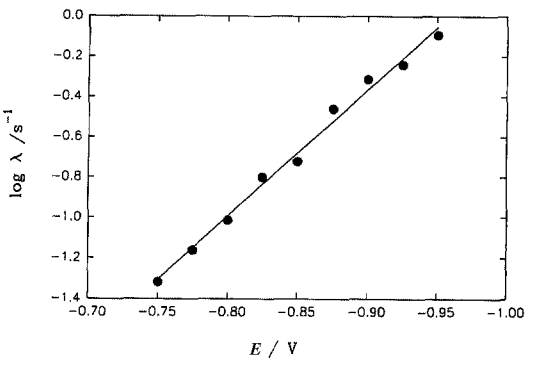

Fig. 14. Dependence of log λ, Equation 12, on applied potential for hard gold deposition at potentials more negative than −0.750 V.

Apparently, this may be attributed to a partial surface coverage by an inhibitor. As the surface coverage by an inhibitor increases and reaches saturation, growth rate decreases with time to a constant value.

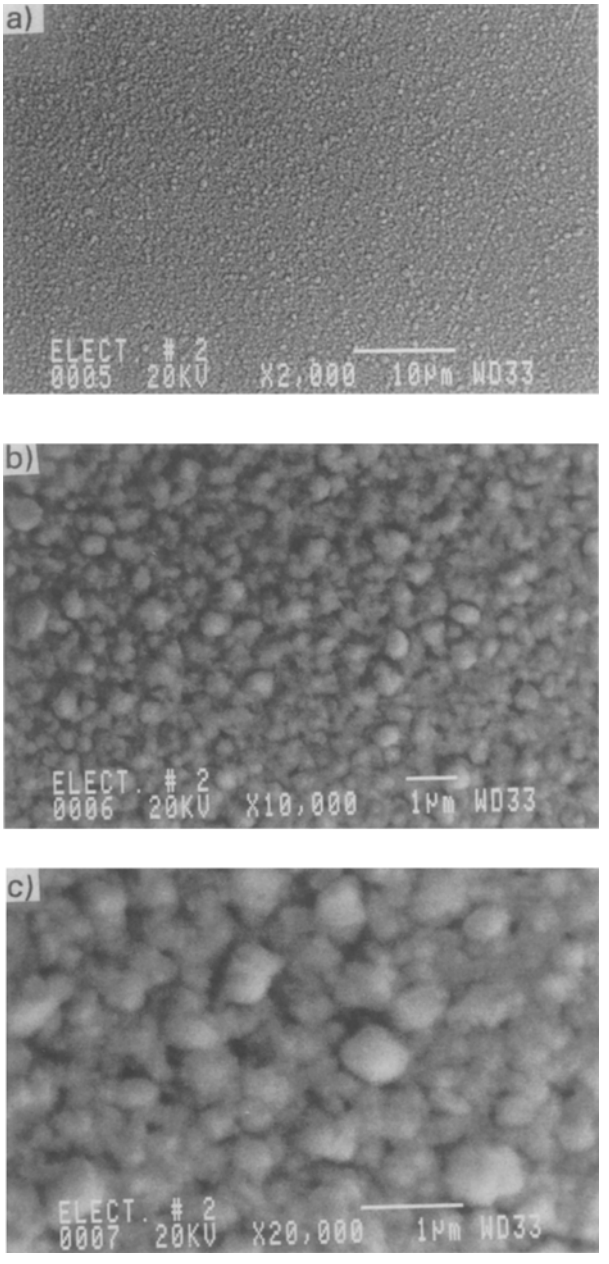

Fig. 15. SEM of hard gold deposits at −0.65 V after 250 s. Magnification: (a) 2000×, (b) 10 000×, and (c) 20 000×.

There are some possibilities for the time-dependent inhibition of vertical growth, for example, the adsorption of nickel and hydrogen. In the electrocrystallization of nickel, H_{ads} causes inhibition of nickel crystal growth [39, 40]. Intermediate $NiOH_{ads}$ is also claimed to inhibit the nickel deposition [40].

Another plausible explanation for such time-dependence of vertical growth is a simultaneous growth of two phases during the deposition. It is possible that the vertical growth rate for one growing phase decreases with time to zero and another is constant. During nickel electrocrystallization, indeed, Fleischmann and Saraby-Reintjes [41] found that α-Ni, which is defined as a solid solution of hydrogen in nickel, was codeposited simultaneously with β-Ni phase, which is an interstitial hydrogen alloy of nickel with an atomic ratio H/Ni exceeding 0.6. In this case the maximum on current–time transients was caused by the codeposition of β-Ni, whose growth rate was time-dependent. It is possible that two growing phases may be involved in the hard gold deposition. The maximum is probably attributed to the one phase whose vertical growth rate is time-dependent, and the steady-state may be caused by another phase whose vertical growth rate is constant.

The results obtained lead us to conclude that two mechanisms are involved in both hard gold and soft gold deposition from Renovel N acid solutions. At more positive potentials, similar to the soft gold deposition, a self-inhibition process occurs in hard gold deposition. It is worth noticing that so-called self-inhibition phenomenon is a potential rather than time-dependent process: that is, in this potential range, the growth rate of 3D crystals is constant at each potential, however, the inhibition of vertical growth is observed with an increase in negative potential. Such inhibition phenomenon is probably connected with the production of CN^- or HCN species on the electrode surface as well as adsorption of other unknown inhibitors [23]. The largest difference between soft and hard gold deposition processes results from the deposition at more negative potentials. Due to the presence of nickel, current for hard gold is much lower than that for soft gold, indicating that crystal growth is retarded. A maximum-like behaviour of current–time transient may be related to a nucleation and growth process with partial inhibition which might be caused by a time dependent partial coverage by an inhibitor or two different growing phases.

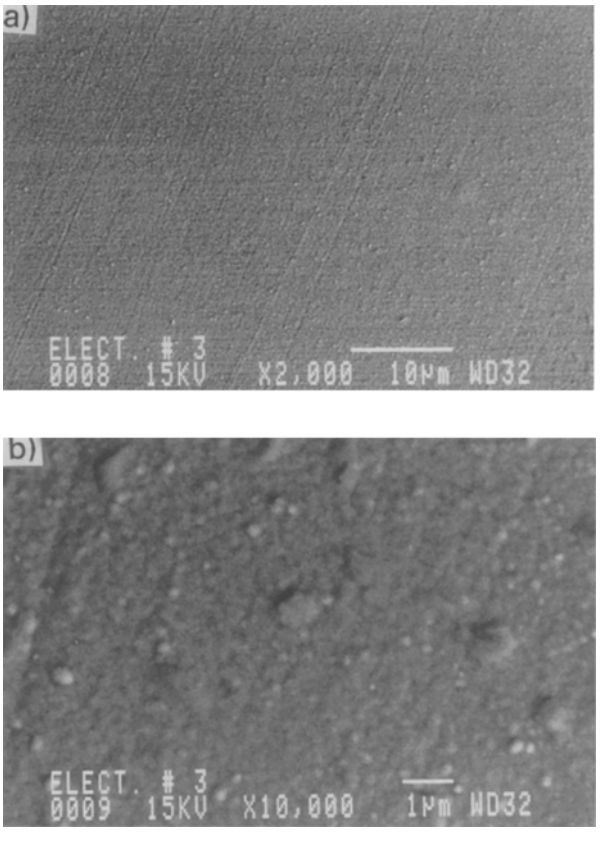

Fig. 16. SEM of hard gold deposits at −0.9 V after 120 s. Magnification: (a) 2000× and (b) 10 000×.

5.3. *Morphology of deposits*

Deposits obtained exhibit different appearance at different potentials. Bright and smooth deposits were observed at potentials more positive than peak potential on the LSVs, both for soft and hard gold deposits. Surface changed from bright to dull as potential became more negative than peak potential, due to inhibition of vertical growth. In a second potential region, deposits were usually bright and smooth.

Figure 15 shows SEM pictures of hard gold deposited at −0.65 V for 250 s. This represents a typical measurement in a more positive potential range. A large number of nearly hemispherical granular crystalline growth with different polygonal crystals are seen distributed randomly on the surface of thin deposit. Since during the deposition time of 250 s current reached a quasi-plateau, Fig. 3(a), overlaps of adjacent growing crystals are observed in Fig. 15. The grain size of crystals varies, as clearly seen in Fig. 15(c). This indicates that nucleation is progressive, as suggested previously in the model (Equation 11).

Figure 16 shows the surface morphology of hard gold deposited at −0.90 V for 150 s. This measurement is an example of deposition in more negative potential range. Two growing phases are revealed from the SEM micrographs, Fig. 16(b): that is, the distribution of grain size is bimodal, one phase consists of large number of uniform and small crystals and the other contains bigger grains. Such a bimodal distribution of grain sizes was also observed by Pindra *et al.* [20] during hard gold deposition, the growth of Au–Ni crystals was partially inhibited. Hence, the partial inhibition model proposed in this work seems reasonable.

Besides, the influence of nickel and/or non-metallic inclusions may also play a role on the nucleation and crystal growth. Nakahara [16] studied morphology of the cobalt hardened gold deposits in acid solution by means of SEM and TEM, and found similar hemispherical structure, so-called 'rounded mound'

growth. Accordingly, the 'rounded mound' growth consists of extremely fine gold grains, the nucleation of which was accompanied by the incorporation of numerous nonmetallic molecules, which may act as growth inhibitors. Although nonmetallic inclusions in nickel hardened gold deposits were not yet identified, a similar effect as that for cobalt hardened gold might be expected, that is, inhibition of growth in certain direction may be resulted from the nonmetallic inclusion in the deposits.

6. Conclusions

The mechanism of hard gold deposition from Renovel N bath is similar to that for soft gold, that is, adsorption of AuCN followed by a charge-transfer step in a more positive potential range and a direct charge-transfer reaction mechanism at more negative potentials. Tafel slopes in these two regions are higher than those for soft gold.

A self-inhibition phenomenon, which was observed during soft gold deposition at more positive potentials, was further confirmed for hard gold by linear sweep voltammetric and chronoamperometric experiments. A simple model of three-dimensional progressive nucleation and growth of right-circular cones was used to interpret the experimental current–time transients recorded in potential range of -0.50 to -0.70 V. The parameters of k_0, k', k^2A_{3D} and A_{3D} were obtained. The growth rate constant for hard gold is much smaller than that for soft gold deposition, indicating that gold deposition process is slowed down by the presence of nickel. Nucleation rate A_{3D} increases with negative potential, contrary to that for soft gold deposition.

A modified Bosco–Rangarajan inhibition model was derived to explain the experimental current-time transients recorded at more negative potentials from -0.75 to -1.0 V. The nucleation and crystal growth mechanism for hard gold deposition in this potential range is well described by a model of three-dimensional instantaneous nucleation and crystal growth with time-dependent inhibition in vertical direction. Vertical growth rate was assumed to decrease exponentially with time to a constant value. The parameters of k_0, k_1, k_2 and k^2N_0 were determined.

Acknowledgements

Financial support from NSERC is gratefully acknowledged.

References

[1] W. T. Lee, *Corros. Technol.* **10** (1963) 4.
[2] J. A. Lochet, Proceedings of the 77th AESF Annual Technical Conference, Vol. 2 (1990) p. 983.
[3] J. Hendriks, 'Connectors 91', a one day symposium and exhibition (edited by G. D. Wilox and D. H. Ross) Inst. Met. Finishing, Birmingham (1991) p. 20.
[4] H. R. Khan, M. Baumgärtner and Ch. J. Raub, Proceedings of a Symposium Electrodeposition Technology, Theory and Practice, The Electrochemical Society, Pennington NJ (1987) p. 165.
[5] F. R. Schlodder, H. H. Beyer and W. G. Zilske, 'GOLD 100', Proceedings of the International Conference on Gold, Johannesburg, Vol. 3 (1986) p. 21.
[6] S. J. Hemsley and R. V. Green, *Trans. Inst. Metal Finish.* **69** (1991) 149.
[7] C. Bocking and C. Dineen, *ibid.* **72** (1994) 101.
[8] C. Bocking and B. Cameron, *ibid.* **72** (1994) 33.
[9] N. N. Balashova, T. A. Smirnova, N. A. Smagunova and A. K. Yudina, *Zh. Prikl. Khim.* **50** (1977) 2698.
[10] R. M. Krishnan, S. Sriveeraraghavan and S. R. Natarajan, *Metal Finish.* **86** (1988) 56.
[11] J. M. Leeds and M. Clarke, *Trans. Inst. Metal Finish.* **47** (1969) 163.
[12] Y. Okinaka and S. Nakahara, *J. Electrochem. Soc.* **123** (1976) 1284.
[13] R. L. Cohen, F. B. Koch, L. N. Schoenberg and K. W. West, *ibid.* **126** (1979) 1608.
[14] M. Yuasa, Y. Ohtani, I. Sekine and S. Yarita, *Hyomen Gijutsu* **45** (1994) 91.
[15] S. Nakahara, *J. Cryst. Growth* **75** (1986) 212.
[16] C. J. Raub, H. R. Khan and M. Baumgärtner, *Gold Bull.* **19** (1986) 70.
[17] E. T. Eisenmann, *J. Electrochem. Soc.* **125** (1978) 717.
[18] H. Angerer and N. Ibl., *J. Appl. Electrochem.* **9** (1979) 219.
[19] P. Bindra, D. Light, P. Freudenthal and D. Smith, *ibid.* **136** (1989) 3616.
[20] L. Sjögren, B. Asthner, L-G. Liljestrand and L. B. Révay, *Plat. Surf. Finish.* **73** (1986) 70.
[21] I. R. Christie, 'Connectors 91', a one day symposium and exhibition (edited by G. D. Wilox and D. H. Ross) Inst. Met. Finishing, Birmingham (1991) p. 61.
[22] W. Chrazanowski, Y. G. Li and A. Lasia. *J. Appl. Electrochem.*, in press.
[23] Y. G. Li, W. Chrzanowski and A. Lasia, *J. Appl. Electrochem.* **26** (1996) 843–852.
[24] M. Avrami, *J. Chem. Phys.* **7** (1939) 1103; **8** (1940) 212; **9** (1941) 177.
[25] U. R. Evans, *Trans. Faraday Soc.* **41** (1945) 365.
[26] E. Bosco and S. K. Rangarajan, *J. Electroanal. Chem.* **134** (1982) 213, 225.
[27] M. Y. Abyaneh and M. Fleischmann, *J. Electrochem. Soc.* **138** (1991) 2491.
[28] B. Scharifker and G. Hills, *Electrochim. Acta* **28** (1983) 879.
[29] J. Amblard, M. Froment, G. Maurin, N. Spyrellis and E. Trevisan-Souteyrand, *ibid.* **28** (1983) 909.
[30] M. Fleischmann, G. Sundholm and Z. Q. Tian, *ibid.* **31** (1986) 907.
[31] P. M. Rigano, C. Mayer and T. Chierchie, *ibid.* **35** (1990) 1189.
[32] R. D. Armstrong, M. Fleischmann and H. R. Thirsk, *J. Electroanal. Chem.* **11** (1966) 208.
[33] R. G. Barradas, F. C. Benson and S. Fletcher, *ibid.* **80** (1977) 305.
[34] V. G. Roev and N. V. Gudin, *Elektrokhimiya* **31** (1995) 532.
[35] A. Milchev and S. Stoyanov, *J. Electroanal. Chem.* **72** (1976) 33.
[36] A. Milchev and E. Vassileva, *ibid.* **107** (1980) 337.
[37] M. Fleischmann, M. Labram and C. Gabrielli, *Surf. Sci.* **101** (1980) 583.
[38] M. Y. Abyaneh and M. Fleischmann, *J. Electroanal. Chem.* **119** (1981) 197.
[39] E. Chassaing, M. Joussellin and R. Wiart, *ibid.* **157** (1983) 75.
[40] E. Vallés, R. Pollina and E. Gómez, *J. Appl. Electrochem.* **23** (1993) 508.
[41] M. Fleischmann and A. Saraby-Reintjes, *Electrochim. Acta* **31** (1986) 907.

Appendix A

Assuming that $p(t)$ and $q(t)$ are growth rates in the lateral and vertical directions, respectively, and the number of nuclei is N (cm^{-2}), Bosco and Rangarajan [26] showed that the Avrami extended area without

overlap at a height h and after time t is given as

$$S_{X,h} = \pi \int_0^s \mathrm{d}\tau \left(\frac{\mathrm{d}N}{\mathrm{d}t}\right)_\tau \left(\int_w^t p(u)\mathrm{d}u\right)^2 \quad \text{(A1)}$$

where τ is the time at which the centre nucleated, w the time at which the vertical growth attains the height h. Variables s and w both are functions of height h and time t, where

$$h = \int_s^t q(u)\mathrm{d}u = \int_\tau^w q(u)\mathrm{d}u \quad \text{(A2)}$$

The total volume of the deposit is

$$V = \int_0^t q(s)[1 - \exp(-S_{X,h})]\mathrm{d}s \quad \text{(A3)}$$

Differentiation of Equation A3 leads to calculation of the current:

$$i = \frac{zF\rho}{M}\frac{\mathrm{d}V}{\mathrm{d}t} \quad \text{(A4)}$$

In the derivation of the modified Bosco–Rangarajan inhibition model, an instantaneous nucleation is considered, that is, $\mathrm{d}N/\mathrm{d}t = N_0\delta(t)$, where $\delta(t)$ is the Dirac δ function. Provided that lateral growth velocity k (mol cm^{-2} s^{-1}) is constant and vertical growth velocity k' (mol cm^{-2} s^{-1}) is given by Equation 6:

$$k' = k_1 \exp(-\lambda t) + k_2 \quad \text{(A5)}$$

the extended surface area $S_{X,h}$ becomes

$$S_{X,h} = \pi \int_0^s \mathrm{d}\tau N_0\delta(\tau)\left(\int_w^t \frac{Mk}{\rho}\mathrm{d}u\right)^2 = P_2(t-w)^2 \quad \text{(A6)}$$

where $P_2 = \pi M^2k^2N_0/\rho^2$. From Equation A3, the volume, V, is expressed as

$$V = \int_0^t \frac{M}{\rho}[k_1\exp(-\lambda s) + k_2][1 - \exp(-P_2(t-w)^2)]\mathrm{d}s \quad \text{(A7)}$$

Differentiation of Equation A2, taken t and τ as constants, leads to

$$q(s)\mathrm{d}s = -q(w)\mathrm{d}w \quad \text{(A8)}$$

and

$$\mathrm{d}s = -\frac{q(w)}{q(s)}\mathrm{d}w = -\frac{k_1\exp(-\lambda w) + k_2}{k_1\exp(-\lambda s) + k_2}\mathrm{d}w \quad \text{(A9)}$$

Therefore, Equation A7 becomes:

$$V = \int_0^t \frac{M}{\rho}[k_1\exp(-\lambda w) + k_2][1 - \exp(-P_2(t-w)^2)]\mathrm{d}w = \frac{Mk_1}{\rho}\int_0^t \exp(-\lambda w)[1 - \exp(-P_2(t-w)^2)]\mathrm{d}w + \frac{Mk_2}{\rho}\int_0^t [1 - \exp(-P_2(t-w)^2)]\mathrm{d}w \quad \text{(A10)}$$

The current, Equation A4, is expressed as

$$i = zFk_1\left[\exp(-\lambda t) - \exp(-P_2t^2) + \lambda\exp(-\lambda t) \times \int_0^t \exp(-P_2u^2 + \lambda u)\mathrm{d}u\right] + zFk_2[1 - \exp(-P_2t^2)] \quad \text{(A11)}$$

In Equation A11, current consists of two terms, the first term was given in [26] (Equation 4) in which vertical growth rate was defined by Equation 3 with $n = 1$; the second term actually is the current equation derived by Armstrong *et al.* [32] for 3D instantaneous nucleation and growth of right-circular cones with vertical growth rate constant k_2 and lateral growth rate constant k. It should be mentioned that equations developed in [32] for both instantaneous or progressive nucleation and growth of right-circular cones with constant growth rate in two directions can also be derived using the general model of Bosco and Rangarajan [26].

Appendix B

Other models for partial inhibition of the vertical growth, Equation 5, may be similarly derived. Provided that vertical growth velocity is

$$k' = k_1\exp(-\lambda t^2) + k_2 \quad \text{(B1)}$$

For instantaneous nucleation, the extended area is

$$S_{X,h} = \pi \int_0^s \mathrm{d}\tau N_0\delta(\tau)\left(\int_w^t \frac{Mk}{\rho}\mathrm{d}u\right)^2 = P_2(t-w)^2 \quad \text{(B2)}$$

and volume is

$$V = \frac{Mk_1}{\rho}\int_0^t \exp(-\lambda w^2)[1 - \exp(-P_2(t-w)^2)]\mathrm{d}w + \frac{Mk_2}{\rho}\int_0^t [1 - \exp(-P_2(t-w)^2)]\mathrm{d}w \quad \text{(B3)}$$

By differentiating of B3, the current becomes

$$i = 2zFk_1P_2\int_0^t (t-w)\exp(-\lambda w^2)\exp(-P_2(t-w)^2\mathrm{d}w + zFk_2[1 - \exp(-P_2t^2)] \quad \text{(B4)}$$

Equation B4 also consists of two term. First term corresponds to the case in which vertical growth rate is defined by Equation 3 with $n = 2$. Notice that some parameters were missing in the equation given in [26]. Second term in Equation B4 corresponds to 3D instantaneous nucleation and growth of right-circular cones, as discussed above.